Project 1, TMA4320: Gravity Surveying

Nils Petter Jørstad, 480441, nilspj
Elisabeth Thrane, 478701, elisasth

February 8, 2021

1 Introduction

In this document, we present our answers and results to the questions in Project 1. Furthermore, we will discuss whether our results adhered to our expectations and are reasonable.

2 Measurement model

2.1 Question 1

By calculating the antiderivative of the kernel $K(x, y)$ from equation (8) on the interval $I = [0, 1]$, we managed to calculate the force $F(x)$ from equation (6) as a function of x. As we can see from the plot, the larger the depth d, the less variation in the measurements there are. When $d_3 = 2.5$ m the plot is almost a flat line, while when $d_1 = 0.025$ m, the plot has a huge variation from below 10^{-1} N to almost 10^2 N. The results in Figure (1) are not surprising because from Newtons law of universal gravitation, we know that the force $F(x)$ is inversely proportional to the distance squared (d^2). So as the distance increases, the force ultimately becomes weaker. However, at the same time, we can claim that the error in the measurements become greater when the distance increases. We know from the project document that $\rho(x)$ is equal to 1 on the interval $[\frac{1}{3}, \frac{2}{3}]$, and 0 otherwise. When $d_1 = 0.025$ m, we see from the Figure (1) that the force is constant in that interval. When the depth increases, this straight line becomes more and more curved on $[\frac{1}{3}, \frac{2}{3}]$. This means that the force measurements become less exact, and therefore has greater error.

3 Spectral collocation discretization of (6)

3.1 Question 2

By doing what the exercise suggested, we split up the Fredholm integral equation of the first kind (6) into discrete sums that the computer can calculate by substituting equation (9) and (11) into (6). Each element of the force F corresponding to a collocation point x_i^c, can then be written as

$$F(x_i^c) = \sum_{i=0}^{N_c-1} K(x_i^c, x_k^q) w_k \sum_{j=0}^{N_s-1} \hat{\rho}_j L_j(x_k^q), \tag{1}$$

where x_k^q and w_k are the quadrature nodes and weights respectively for $k = 0, 1, ..., N_q - 1$, and L_j is from equation (10). We can identify the vectors $\hat{\boldsymbol{\rho}} = [\hat{\rho}_0, ..., \hat{\rho}_{N_s-1}]^{\mathrm{T}} \in \mathbb{R}^{N_s}$ and $\boldsymbol{b} = [F(x_0^c), ..., F(x_{N_c-1}^c)]^{\mathrm{T}} \in \mathbb{R}^{N_c}$ in this equation (1) and rearrange the equation such that it has the form,

$$\mathbf{A}\hat{\boldsymbol{\rho}} = \mathbf{b}. \tag{2}$$

From this we can express the matrix A with

$$A = \sum_{i=0}^{N_c-1} K(x_i^c, x_k^q) w_k \sum_{j=0}^{N_s-1} L_j(x_k^q), \tag{3}$$

and furthermore we can write each element of A in terms of the kernel $K(x, y)$, x_i^c, x_j^s, x_k^q and w_k with

$$A_{ij} = \sum_{k=0}^{N_q-1} K(x_i^c, x_k^q) w_k L_j(x_k^q) = \sum_{k=0}^{N_q-1} K(x_i^c, x_k^q) w_k \frac{\prod_{m \neq j}(x_k^q - x_m^s)}{\prod_{m \neq j}(x_j^s - x_m^s)}, \tag{4}$$

where in the last equality L_j is replaced with its definition in equation (10).

3.2 Question 3 and 4

By using a test density $\rho(x) = \sin(\omega x)\exp(\gamma x)$ and a corresponding analytical test $F(x)$, the accuracy of A was tested for midpoint Newton-Côtes quadrature and Legendre-Gauss quadrature on interval $[a, b]$. The maximum element of the error vector $|F(x_i^c) - (A\hat{\rho})_i|$ was calculated for different values of x_k^q and w_k given by N_q panels and plotted as a function of N_q. The resulting plot in Figure (2) shows that the Legendre-Gauss quadrature converges substantially faster than the Newton-Côtes method when the number of panels increases. To know why this is the case, we have to look at the degree of precision of both methods.

The definition of the degree of precision of a quadrature formula is the largest positive integer n such that the formula is *exact* for x^k for each $k = 0, 1, 2, ..., n$ [1]. In other words, the degree of precision of a method is equal to n if and only if the error is zero for all polynomials of degree $k = 0, 1, 2, ..., n$, but is not zero for some polynomial of degree $n + 1$ [1]. Theorem 5.6 in *Numerical Analysis* states that the Legendre-Gauss quadrature method, using the degree n Legendre polynomial on $[-1, 1]$ has degree of precision $2n - 1$ when $n + 1$ points are used [1]. This also applies to a general interval $[a, b]$. The Newton-Côtes methods only has degree of precision n (for n odd) and $n + 1$ (for n even) for $n + 1$ points [1]. This means that the Legendre-Gauss method has more than double the precision of the midpoint formula which has degree of precision one. This explains its higher rate of convergence.

4 Direct inversion

4.1 Question 5

To find the most exact result, the error between the numerical solution and the true solution, $\max_{0 \leq j \leq N_s - 1} |\hat{\boldsymbol{\rho}}_j - \rho(x_j^s)|$ was computed for sufficient amounts of nodes, collocation and source points. The numerical solution is found by solving the linear algebraic system (2) for vector $\hat{\boldsymbol{\rho}}$. The maximum error was plotted as a function of N_c for three different values of depth $d_{i=1,2,3}$. For simplicity, the amount of source points is the same as collocation points. To get maximum possible accuracy, the amount of Legendre-Gauss quadrature nodes was set to $N_q = N_c^2$. The plot in Figure (3) shows that the error doesn't converge for all values of d. The smallest depth d_1 gives a satisfyingly small error when N_c increases. The depth d_2 error decreases alongside d_1 until $N_c = 15$ and then increases back to over it's starting value. The d_3 error increases dramatically to begin with and ends up at an error of about 10^9.
So why do the graphs behave like this? From Question 1 we looked at the Fredholm integral equation of the first kind and learned that the variation in force measurement $F(x)$ is related to the variation in density ρ. From Figure (1), we see that $F(x)$ varies for different values of depth d. The error in $F(x)$ when $d_3 = 2.5$ m is especially large, and decreases significantly when d decreases. Since the force measurement $F(x)$ and the density ρ are closely related, this means that the solution to the equation (2) will vary greatly for different values of d. This explains why the error for d_3 in Figure (2) grows and is large, because the error in the measurements are large.
When it comes to explaining why the error in d_2 increases after $N_c = 15$, we learned from the project document that this method of solving a linear system of equations *exactly* has an infinite error amplification factor. This means that this method of finding the solution $\hat{\boldsymbol{\rho}}$ only works up to a certain point until it blows up and gives us values that are too large.

4.2 Question 6

To model real-life situations, the left hand side of the system (2) was perturbed with small random errors between $\pm 0.1\%$ of the measurements. With $N_c = N_s = 30$ and different depths $d_{i=1,2,3}$, the perturbed $\boldsymbol{b}$ and non-perturbed $\tilde{\boldsymbol{b}}$ left hand sides were plotted as functions of x. The solutions of (2) for both $\boldsymbol{b}$ and $\tilde{\boldsymbol{b}}$ were also plotted, along with the analytical solution $\rho(x)$ for comparison for all d. In Figure (4) we can see that the error amplification of the inverse problem isn't too significant for the smallest value d_1, since the the graphs overlap fairly accurately. In Figure (5) the error amplification is very significant for the perturbed solution for d_2, especially in the end points where the values go up to $2 \cdot 10^7$ kg/m^3. The error between the endpoints lies in the range 10^4 to 10^6. The non-perturbed solution is relatively accurate when the limit of the y-axis was set to $[1, 1]$, which we have seen and tested. Figure (6) shows even greater error amplification for both the perturbed and non-perturbed solutions with d_3. The results from both Figure (5) and Figure (6) are unsatisfactory, because we have produced large and possibly useless answers $\hat{\boldsymbol{\rho}}$. The reason for this is the same as in Question 5, because when solving a system of linear equations exact, the error amplification factor becomes infinite.

5 Tikhonov regularization

5.1 Question 7

When using Tikhonov regularization one has to solve the equation,

$$(\boldsymbol{A}^{\mathrm{T}}\boldsymbol{A} + \lambda \boldsymbol{I})\hat{\boldsymbol{\rho}} = \boldsymbol{A}^{\mathrm{T}}\tilde{\boldsymbol{b}}, \tag{5}$$

where $\lambda > 0$, $\boldsymbol{I}$ is the identity matrix and $\tilde{\boldsymbol{b}}$ is the perturbed $\tilde{F}(x_c^i)$ vector. In Figure (7) and (9), we plotted the error $\max_j |\rho(x_j^s) - \hat{\boldsymbol{\rho}}_j|$ for d_2 and d_3 to find the best suited λ to solve equation (5). The minimum point on these graphs gives us the smallest error in $\max_j |\rho(x_j^s) - \hat{\boldsymbol{\rho}}_j|$, which is desirable. We want a small error in the solution $\hat{\boldsymbol{\rho}}$. By identifying which λ corresponded to the minimum point, was how we found the best suited λ. For $d_2 = 0.25$ m, we observe from Figure (7) that $\lambda = 10^{-4}$ results in the smallest error. For $d_3 = 2.5$ m, $\lambda = 10^{-9}$ gave the smallest error which we observed from Figure (9).
We then plotted the regularized solution $\hat{\boldsymbol{\rho}}$ with the smallest error (and corresponding λ) and compared it to the analytical solution $\rho(x)$. This was done for depths d_2 and d_3 and he results can be seen in Figure (8) and (10) respectively. The regularized solution in Figure (8) for d_2 follows the analytical solution almost perfectly. It deviates slightly when $x < 0.4$ m, but then stays on track otherwise. This result is more satisfactory than what we presented in Question 6 for d_2, where the error was very large when x approached either 0 or 1 m. In Figure (10), we see that the regularized solution deviates more from the analytical

$\rho(x)$ for d_3 than for d_2. The regularized plot does not follow the analytical plot closely, but they do have a similar shape. This could be because the perturbed $\tilde{F}(x)$ still has a large error for d_3, and therefore affects our regularized $\hat{\boldsymbol{\rho}}$ by increasing its error. Even though we use Tikhonov regularization, this relation between F and ρ is overpowering. However, if we compare Figure (10) to the results for d_3 in Question 6, it is clear that using Tikhonov regularization reduces this error immensely to give us a more satisfactory result, even though it is far from perfect.

6 Reconstruction from given measurements

6.1 Question 8

In the previous questions, an analytical test $\rho(x)$ has been used to find the most accurate solution method by being used as a comparison. Instead, in this question, the Tikhonov regularization method is implemented on three different samples of measured gravitational force and our goal is to find the density distribution for each of them. From the project document, we know that the samples consist of a harmonic wave, a Gaussian and a "square window", each with their own values of depth d. λ for each sample was chosen in the same manner as in Question 7, by choosing the λ that gave the smallest error of $\hat{\boldsymbol{\rho}}$ for each value of d. The reconstructed density of each sample can be seen in Figure (11). Graph 1 and 2 clearly resemble a harmonic wave and a Gaussian, both satisfy our expectations. Graph 3 is the least satisfactory one, but is not too far from resembling a square to be deemed unsatisfactory.

References

[1] T. Sauer, Numerical Analysis, Addison-Wesley Publishing Company, 2nd ed., 2011.

7 Equations from the project document

$$F(x) = \int_a^b K(x,y)\rho(y)dy, \tag{6}$$

$$K(x,y) = \frac{d}{(d^2 + (y-x)^2)^{3/2}} \tag{7}$$

$$\int K(x,y)dy = \frac{y-x}{d(d+(x-y)^2)^{1/2}} \tag{8}$$

$$\rho(x) = \sum_{j=0}^{N_s-1} \hat{\rho_j} L_j(x) \tag{9}$$

$$L_j(x) = \frac{\prod_{m\neq j}(x - x_m^s)}{\prod_{m\neq j}(x_j^s - x_m^s)} \tag{10}$$

$$\int_a^b \phi(z)dz \approx \sum_{k=0}^{N_q-1} \phi(x_k^q) w_k \tag{11}$$

8 Figures

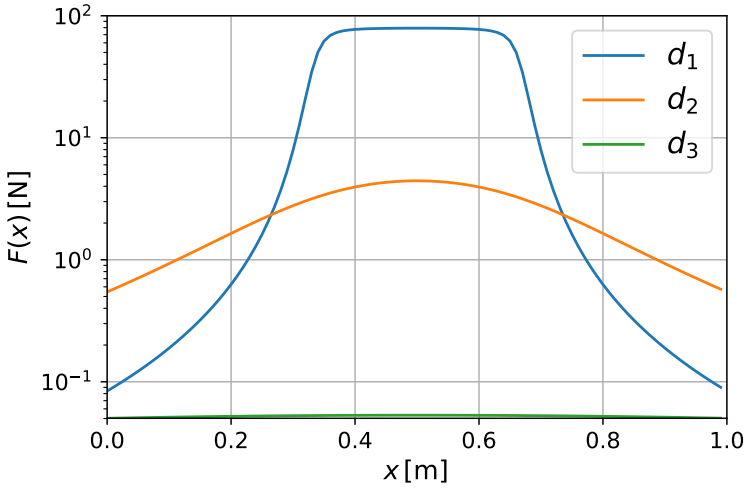

Figure 1: The force measurement function $F(x)$ plotted for different depths, $d_1 = 0.025$ m, $d_2 = 0.25$ m and $d_3 = 2.5$ m, as a function of x with logarithmic scale on the y-axis.

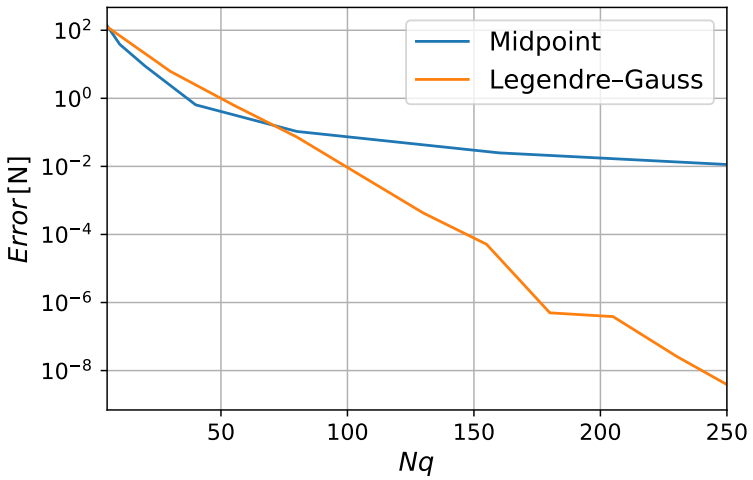

Figure 2: The error $\max_{0 \leq j \leq N_c - 1} |F(x_i^c) - (\boldsymbol{A}\hat{\boldsymbol{\rho}})_i|$ plotted using midpoint Newton-Côtes and Legendre-Gauss methods as a function of N_q panels with logarithmic scale on the y-axis.

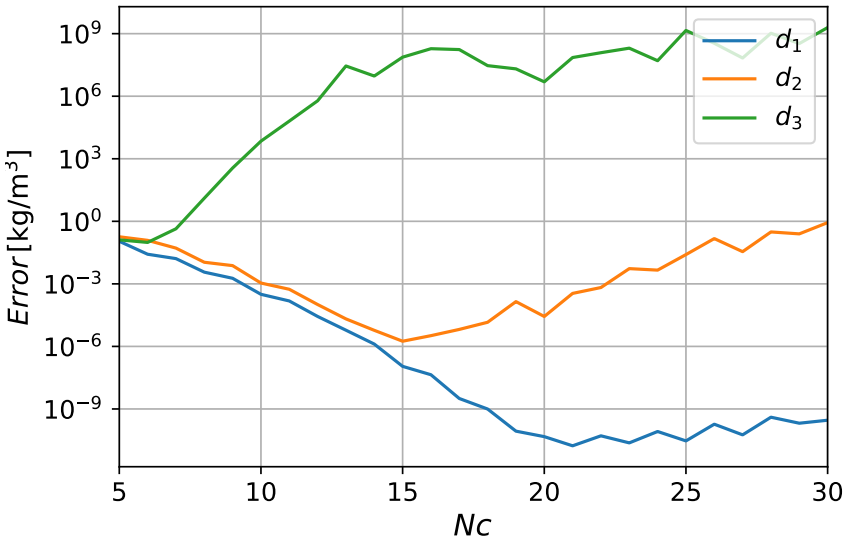

Figure 3: The error $\max_{0\leq j\leq N_s-1}|\hat{\boldsymbol{\rho}}_j - \rho(x_j^s)|$ plotted for different depths, $d_1 = 0.025$ m, $d_2 = 0.25$ m and $d_3 = 2.5$ m, as a function of N_c with logarithmic scale on the y-axis.

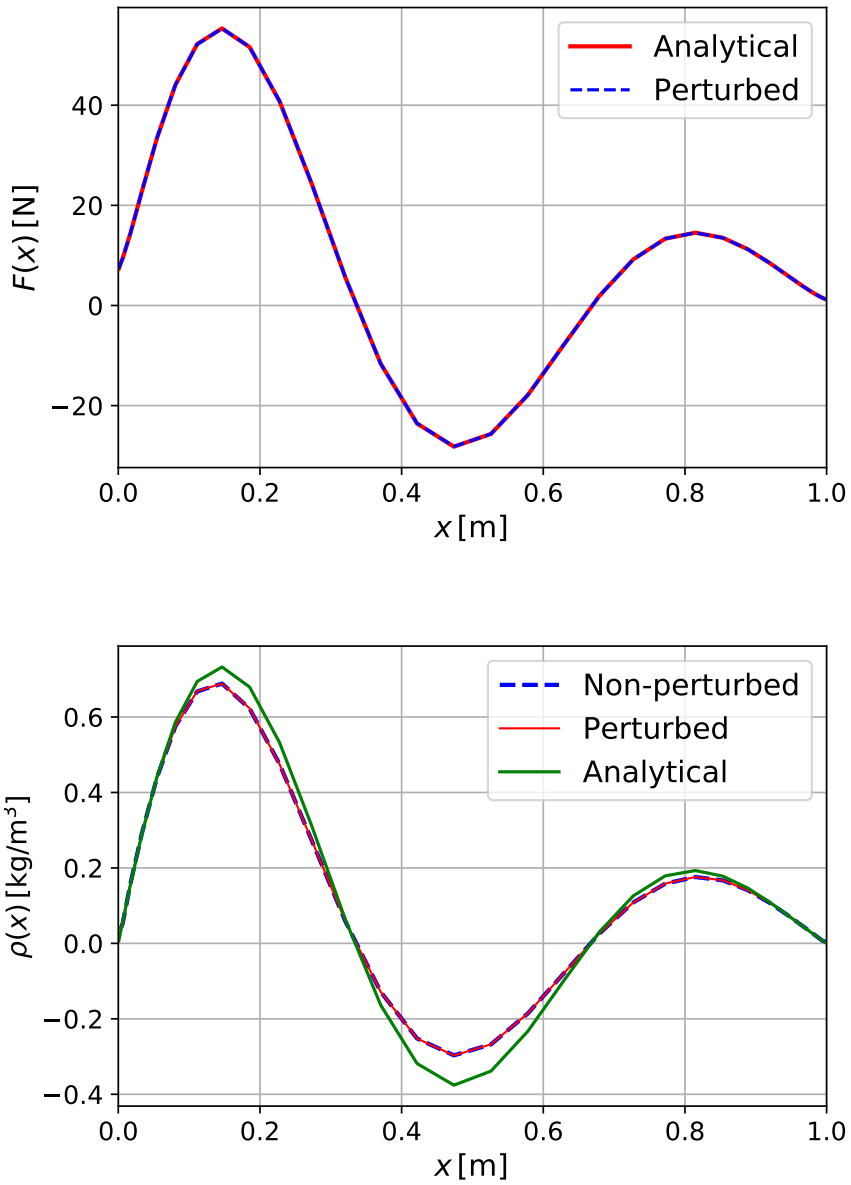

Figure 4: *Above:* The analytical function $F(x)$ plotted against the perturbed function $\tilde{F}(x)$ for depth $d_1 = 0.025$ m as a function of x. *Below:* The analytical function $\rho(x)$ plotted against the perturbed and non-perturbed solutions of equation (2) for depth $d_1 = 0.025$ m as a function of x.

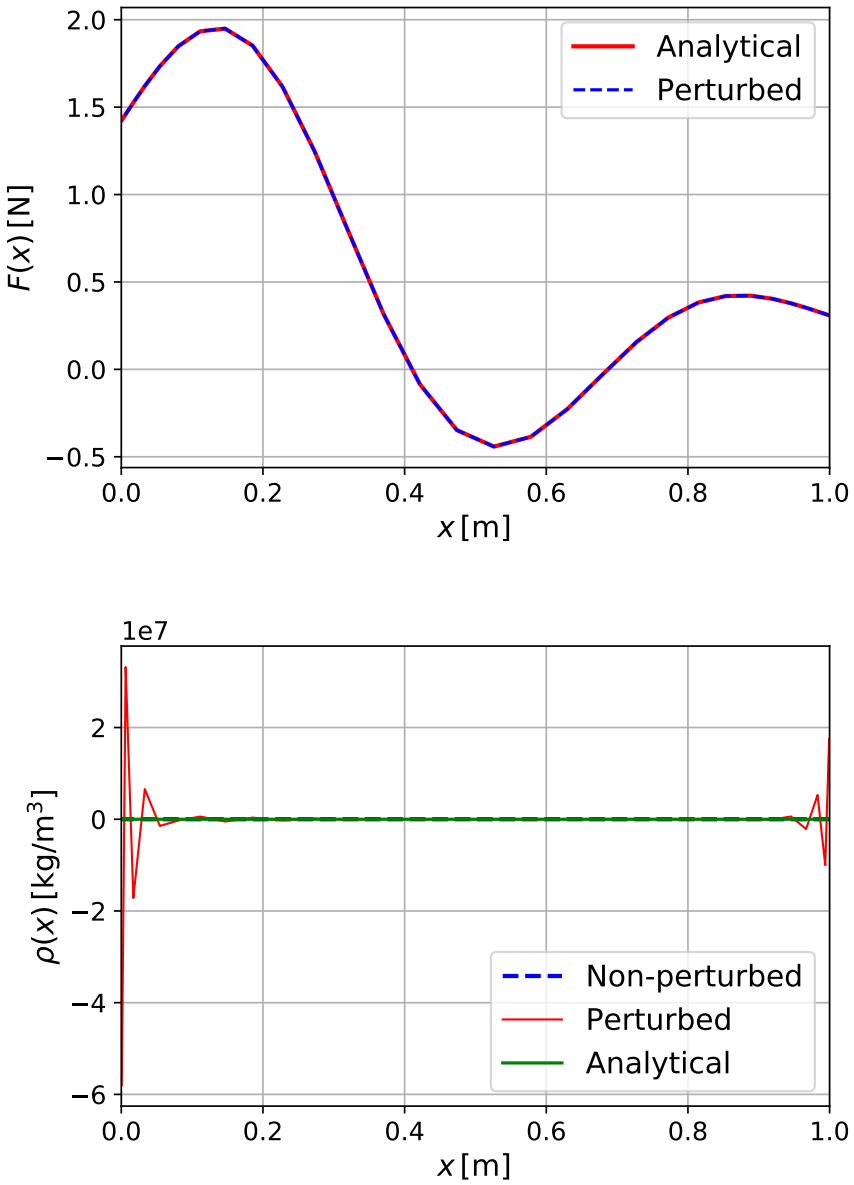

Figure 5: *Above:* The analytical function $F(x)$ plotted against the perturbed function $\tilde{F}(x)$ for depth $d_2 = 0.25$ m as a function of x. *Below:* The analytical function $\rho(x)$ plotted against the perturbed and non-perturbed solutions of equation (2) for depth $d_2 = 0.25$ m as a function of x.

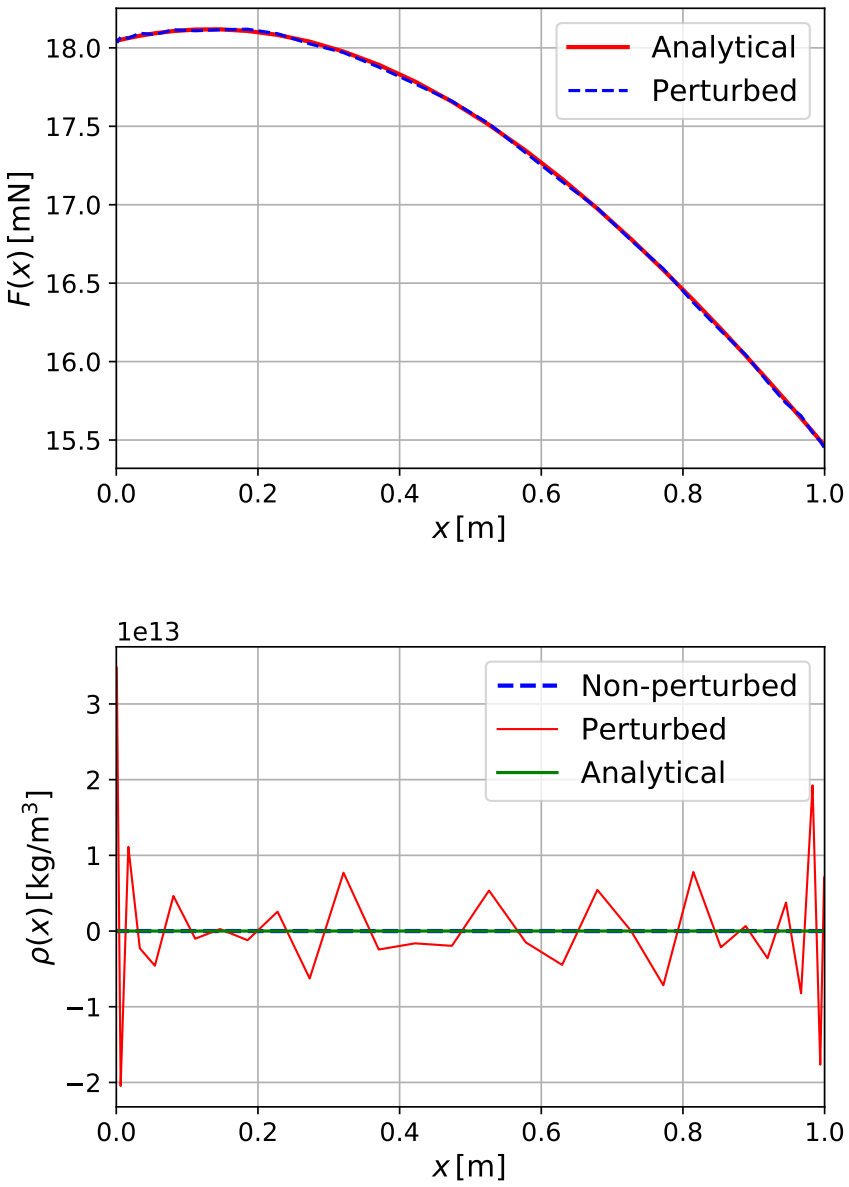

Figure 6: *Above:* The analytical function $F(x)$ plotted against the perturbed function $\tilde{F}(x)$ for depth $d_3 = 2.5$ m as a function of x. *Below:* The analytical function $\rho(x)$ plotted against the perturbed and non-perturbed solutions of equation (2) for depth $d_3 = 2.5$ m as a function of x.

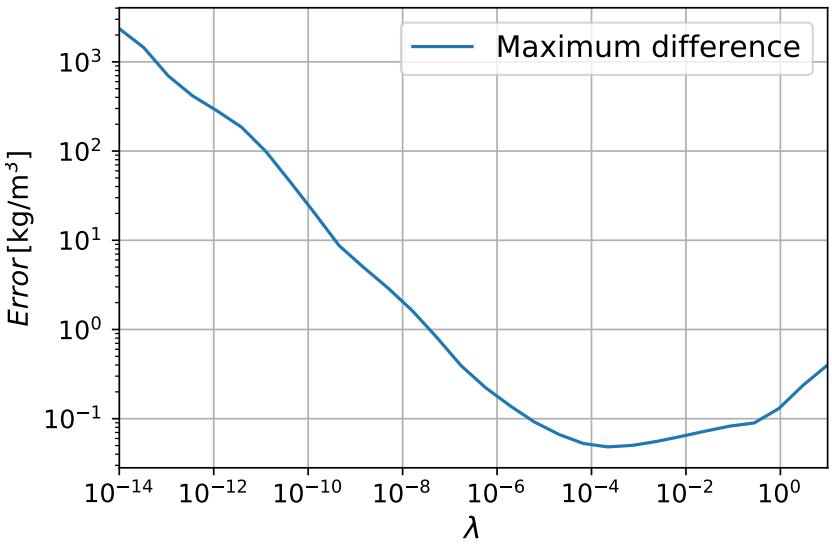

Figure 7: The error $\max_j|\rho(x_j^s) - \hat{\boldsymbol{\rho}}_j|$ plotted for $d_2 = 0.25$ m as a function of λ in the log-log scale.

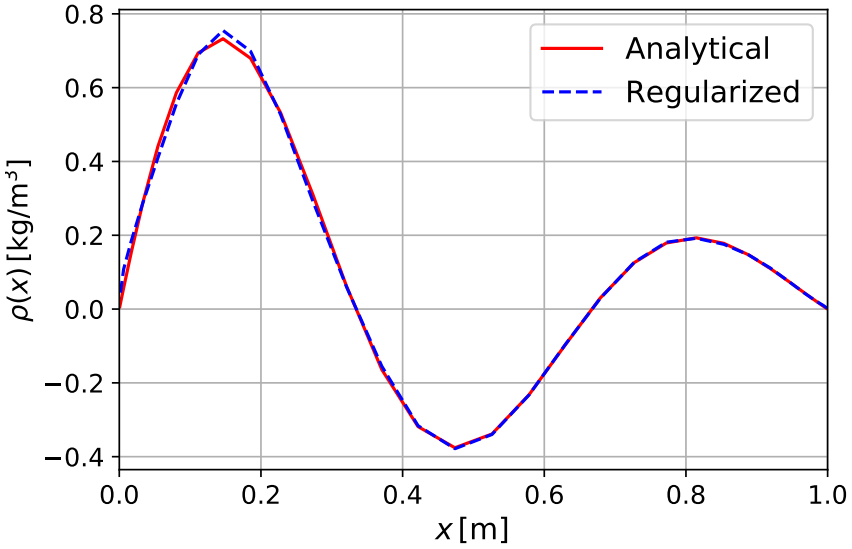

Figure 8: The analytical function $\rho(x)$ plotted against the regularized solution $\hat{\boldsymbol{\rho}}$ from equation (5) for $d_2 = 0.25$ m with $\lambda = 10^{-4}$.

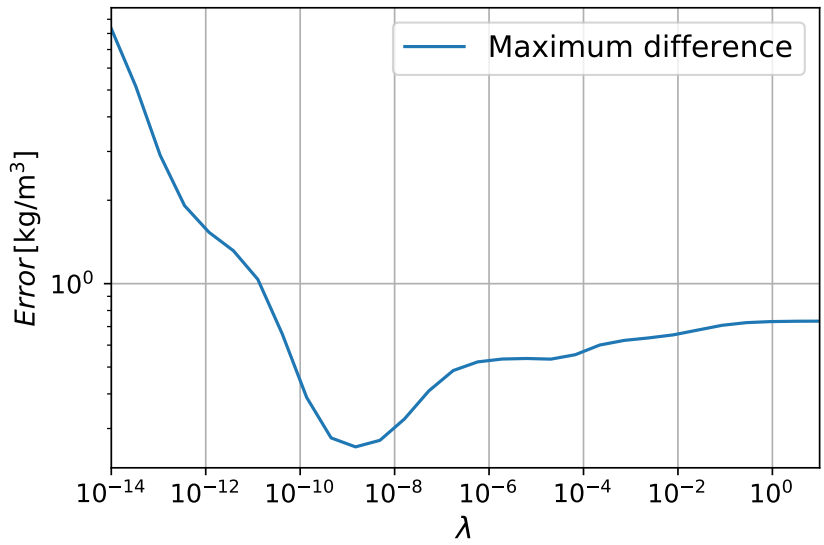

Figure 9: The error $\max_j |\rho(x_j^s) - \hat{\boldsymbol{\rho}}_j|$ plotted for $d_3 = 2.5$ m as a function of λ in the log-log scale.

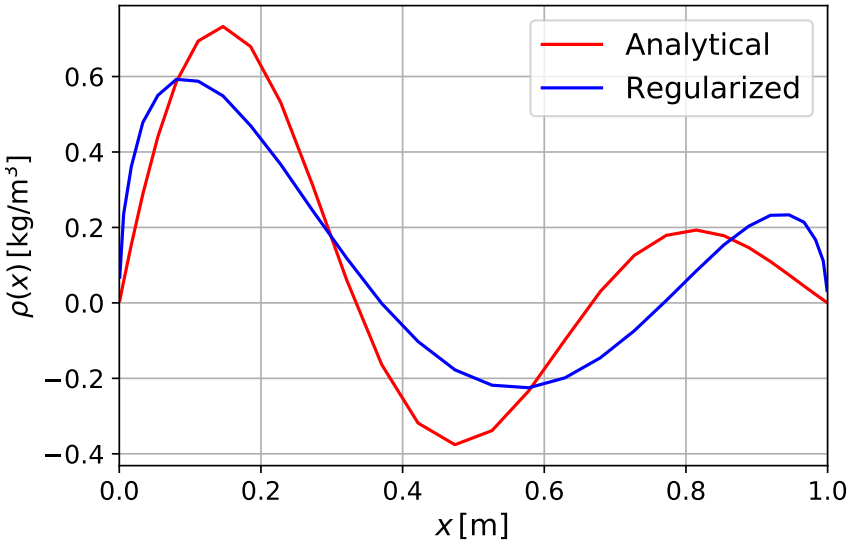

Figure 10: The analytical function $\rho(x)$ plotted against the regularized solution $\hat{\boldsymbol{\rho}}$ from equation (5) for $d_3 = 2.5$ m with $\lambda = 10^{-9}$.

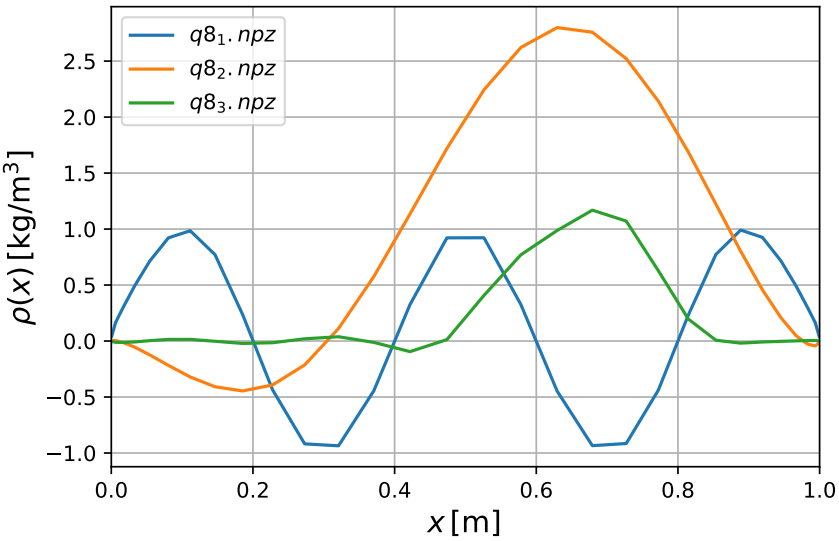

Figure 11: The reconstructed density graphs for the force measurement values in the files: $q8_1$.npz, $q8_2$.npz, $q8_3$.npz.